Quantum electrodynamic description of the neutral hydrogen molecule ionization

Hui-hui Miao*
Faculty of Computational Mathematics and Cybernetics,
Lomonosov Moscow State University, Vorobyovy Gory 1, Moscow, Russia
(Dated: November 27, 2025)

The ionization dynamics of a hydrogen molecule, serving as a fundamental benchmark in quantum chemistry, is investigated within a comprehensive framework combining quantum electrodynamics and the Lindblad master equation. This approach enables a first-principles description of light–matter interactions while accounting for dissipative processes and external particle influx. We systematically explore the system's evolution across three distinct regimes: closed, dissipative open, and influx-driven open quantum systems. Our results reveal a universal tendency towards the formation of the neutral hydrogen molecule ($|H_2\rangle$) across all configurations. The dissipation strengths for photons (γ_Ω), electrons (γ_e), and phonons (γ_ω) are identified as critical control parameters, with γ_Ω significantly accelerating system stabilization. Furthermore, the introduction of particle influx (μ_k) leads to a complex redistribution of energy, notably populating the atomic state ($|H, H\rangle$). The ionization pathway is exquisitely sensitive to the initial quantum state, dictated by the composition and number of photons, which governs the accessible spin-selective excitation channels. This is conclusively demonstrated in a model with an embedded anode, where the maximum ionization probability is fundamentally constrained to $\frac{3}{4}$ by orbital hybridization. This study provides a unified theoretical foundation for quantum-controlled chemistry, with direct implications for future experiments in cavity QED and quantum information processing.

Keywords: hydrogen molecule ionization, finite-dimensional QED, Lindblad master equation, electron

I. INTRODUCTION

The quantum dynamics of chemical processes [1–3], particularly those involving light–matter interactions, represent a frontier in modern physical chemistry. The modeling of chemical reactions related to hydrogen is one of the main objectives of chemical modeling. Numerous theoretical articles [4–9] have recently aroused this interest, namely the positive hydrogen peroxide ion (OH^+) in a thermal bath [6], the neutral hydrogen molecule (H_2) [7, 8], and the hydrogen bond ($O\cdots H$) [9]. Among these, the ionization of the hydrogen molecule stands as a fundamental prototype for understanding electron transfer and bond breaking. While the static electronic structure of H_2 is well-understood, its real-time dynamics under driven and dissipative environments pose significant theoretical challenges. A comprehensive description requires a framework that can simultaneously account for the quantum nature of light, the internal degrees of freedom of the molecule, and the irreversible energy exchange with its surroundings.

Towards this goal, models rooted in the principles of quantum electrodynamics (QED) [10–22]. Many recent studies have advanced the field of QED models, exploring phase transitions [23, 24], quantum many-body phenomena [25, 26], quantum gate implementations [27], and quantum correlations [28, 29]. Further developments include supercomputing realizations of quantum modeling [30, 31]. The QED framework allows for a first-principles description of the interaction between the molecular electrons and the photon field, enabling the precise modeling of phenomena such as stimulated absorption and emission. However, to realistically describe open quantum systems — where dissipation and decoherence are inevitable — the QED Hamiltonian must be coupled with a master equation that governs the system's non-unitary evolution. The Lindblad master equation [32–34] has emerged as the tool for this purpose, providing a mathematically rigorous method to model Markovian dynamics while preserving the positivity of the density matrix ρ.

In this work, we employ a tailored QED model to investigate the ionization dynamics of a hydrogen molecule, described by the Lindblad master equation. Our study systematically explores the system's behavior across three distinct regimes: the coherent, unitary evolution of a closed system; the dissipative dynamics of an open system with particle loss; and the more complex scenario involving the influx of particles. We meticulously analyze the roles of different dissipation channels — for photons, electrons, and phonons — and their impact on the formation of the hydrogen molecular cation (H_2^+). Furthermore, we extend our model to incorporate a built-in anode, providing a novel perspective on the competition between electron escape and molecular stabilization.

Our results delineate the system's inherent propensity to form the H_2, identify key dissipation parameters that either promote or suppress ionization, and reveal how initial quantum state preparation dictates the final outcome. By bridging coherent dynamics, dissipative processes, and external driving, this work offers a unified picture of hydrogen molecule ionization, providing insights that could inform experiments in quantum optics and the control of chemical reactions at the quantum level.

* Correspondence to: Vorobyovy Gory 1, Moscow, 119991, Russia. E-mail address: hhmiao@cs.msu.ru

II. THEORETICAL MODEL

The ionization model of the neutral hydrogen molecule is an extension of our previous association–dissociation model of the neutral hydrogen molecule [7, 8]. In our model, each energy level, whether atomic or molecular, is divided into two states: spin-up (↑) and spin-down (↓). According to the Pauli exclusion principle, each energy level may contain no more than one electron [35]. The schematic diagram of the target model is shown in Fig. 1 (a), where the hybridization of atomic orbitals (0_1 and 0_2) from two hydrogen atoms, results in the formation of two molecular orbitals: a bonding orbital (Φ_0) and an antibonding orbital (Φ_1). These two molecular orbitals take the form

$$\Phi_0 = \frac{1}{\sqrt{2}}\left(0_1 + 0_2\right), \tag{1a}$$

$$\Phi_1 = \frac{1}{\sqrt{2}}\left(0_1 - 0_2\right). \tag{1b}$$

According to Eq. (1), we can obtain

$$0_1 = \frac{1}{\sqrt{2}}\left(\Phi_0 + \Phi_1\right), \tag{2a}$$

$$0_2 = \frac{1}{\sqrt{2}}\left(\Phi_0 - \Phi_1\right). \tag{2b}$$

After the molecular orbital is formed, two electrons with opposite spins, originally belonging to different atoms, occupy these two orbitals and undergo transitions between them through excitation–relaxation processes. Simultaneously, a transitional orbital (Φ_2) exists farther away from the two atomic nuclei, allowing electrons to transition between orbitals Φ_2 and Φ_1 via excitation–relaxation. Taking an electron with ↑ in the antibonding orbital as an example. The electron absorbs a photon of mode $\Omega_{12}^{\uparrow}$ and transitions to the transitional orbital. Given its high energy and increased distance from the nuclei, the electron in the transitional state can be approximated as free electrons that have completely escaped the molecule. An analogous mechanism applies to the spin-down electron. We stipulate that at most one electron can transition to the Φ_2 orbital at any given time.

The Hilbert space of quantum states of the entire system, having the following form

$$|\Psi\rangle = |p_1\rangle_{\Omega_{12}^{\uparrow}}|p_2\rangle_{\Omega_{12}^{\downarrow}}|p_3\rangle_{\Omega_{01}^{\uparrow}}|p_4\rangle_{\Omega_{01}^{\downarrow}}|p_5\rangle_{\omega}|L\rangle_b|k\rangle_n|l_1\rangle_{e^{\uparrow}}|l_2\rangle_{e^{\downarrow}}, \tag{3}$$

where $p_1,\ p_2,\ p_3,\ p_4,\ p_5$ are the numbers of photons of modes $\Omega_{12}^{\uparrow}$, $\Omega_{12}^{\downarrow}$, $\Omega_{01}^{\uparrow}$, $\Omega_{01}^{\downarrow}$, ω, respectively. Here, $\Omega_{12}^{\uparrow}$ is the mode of the photon required for an electron with ↑ to transition from orbital Φ_1 to orbital Φ_2, $\Omega_{12}^{\downarrow}$ is the mode of the photon required for an electron with ↓ to transition from orbital Φ_1 to orbital Φ_2, $\Omega_{01}^{\uparrow}$ is the mode of the photon required for an electron with ↑ to transition from orbital Φ_0 to orbital Φ_1, $\Omega_{01}^{\downarrow}$ is the mode of the photon required for an electron with ↓ to transition from orbital Φ_0 to orbital Φ_1. The state of the covalent bond are denoted by $|L\rangle_b$: $L = 0$ — covalent bond formation, $L = 1$ — covalent bond breaking. The state of the nuclei are denoted by $|k\rangle_n$: $k = 0$ — state of nuclei, gathering together in one cavity, $k = 1$ — state of nuclei, scattering in different cavities. $l_1,\ l_2$ describe the state of electrons: $l_1(l_2) = 0$ — electron with spin ↑ (↓) in the orbital Φ_0, $l_1(l_2) = 1$ — electron with spin ↑ (↓) in the orbital Φ_1, $l_1(l_2) = 2$ — electron with spin ↑ (↓) in the orbital Φ_2, $l_1(l_2) = \varnothing$ — electron with spin ↑ (↓) detaches from the transitional orbital and becomes a free electron.

The dynamics of system is described by solving the Lindblad master equation in the Markovian approximation for the density operator ρ of the system

$$\begin{aligned} i\hbar\dot{\rho} &= [H,\rho] + iL(\rho) \\ &= [H,\rho] + i\left[\sum_{k\in\mathcal{K}} L_k(\rho) + \sum_{k'\in\mathcal{K}'} L_{k'}(\rho)\right] \\ &= [H,\rho] + i\left[\sum_{k\in\mathcal{K}} \gamma_k\left(A_k\rho A_k^{\dagger} - \frac{1}{2}\left\{\rho, A_k^{\dagger}A_k\right\}\right)\right. \\ &\quad \left. + \sum_{k'\in\mathcal{K}'} L_{k'}\gamma_{k'}\left(A_k^{\dagger}\rho A_k - \frac{1}{2}\left\{\rho, A_k A_k^{\dagger}\right\}\right)\right], \end{aligned} \tag{4}$$

where the term γ_k refers to the overall spontaneous emission rate for photons for $k \in \mathcal{K}$. The total spontaneous influx rate for photon for $k' \in \mathcal{K}'$ is denoted by $\gamma_{k'}$. And,

$$[H,\rho] = H\rho - \rho H, \tag{5a}$$

$$\left\{\rho, A_k^{\dagger}A_k\right\} = \rho A_k^{\dagger}A_k + A_k^{\dagger}A_k\rho, \tag{5b}$$

$$\left\{\rho, A_k A_k^{\dagger}\right\} = \rho A_k A_k^{\dagger} + A_k A_k^{\dagger}\rho. \tag{5c}$$

Hamiltonian of the model with consideration of rotation wave approximation (RWA) [36] has following form

$$H = H_{atom} + H_{field} + H_{int} + H_{bond} + H_{tun}, \tag{6}$$

where H_{atom} illustrates the atomic energy, H_{field} shows the cavity field energy, H_{int} depicts the interaction, H_{bond} represents the formation of the covalent bond, H_{tun} represents the tunneling effect. And,

$$\begin{aligned} H_{atom} &= \hbar\Omega_{01}^{\uparrow}\sigma_{\Omega_{01}^{\uparrow}}^{\dagger}\sigma_{\Omega_{01}^{\uparrow}} + \hbar\Omega_{01}^{\downarrow}\sigma_{\Omega_{01}^{\downarrow}}^{\dagger}\sigma_{\Omega_{01}^{\downarrow}} \\ &\quad + \hbar\left(\Omega_{01}^{\uparrow} + \Omega_{12}^{\uparrow}\right)\sigma_{\Omega_{12}^{\uparrow}}^{\dagger}\sigma_{\Omega_{12}^{\uparrow}} \\ &\quad + \hbar\left(\Omega_{01}^{\uparrow} + \Omega_{12}^{\uparrow}\right)\sigma_{\Omega_{12}^{\downarrow}}^{\dagger}\sigma_{\Omega_{12}^{\downarrow}}, \end{aligned} \tag{7a}$$

$$\begin{aligned} H_{field} &= \hbar\Omega_{01}^{\uparrow}a_{\Omega_{01}^{\uparrow}}^{\dagger}a_{\Omega_{01}^{\uparrow}} + \hbar\Omega_{01}^{\downarrow}a_{\Omega_{01}^{\downarrow}}^{\dagger}a_{\Omega_{01}^{\downarrow}} \\ &\quad + \hbar\Omega_{12}^{\uparrow}a_{\Omega_{12}^{\uparrow}}^{\dagger}a_{\Omega_{12}^{\uparrow}} + \hbar\Omega_{12}^{\downarrow}a_{\Omega_{12}^{\downarrow}}^{\dagger}a_{\Omega_{12}^{\downarrow}}, \end{aligned} \tag{7b}$$

$$\begin{aligned} H_{int} &= \left[g_{\Omega_{01}^{\uparrow}}\left(a_{\Omega_{01}^{\uparrow}}^{\dagger}\sigma_{\Omega_{01}^{\uparrow}} + a_{\Omega_{01}^{\uparrow}}\sigma_{\Omega_{01}^{\uparrow}}^{\dagger}\right)\right. \\ &\quad \left. + g_{\Omega_{01}^{\downarrow}}\left(a_{\Omega_{01}^{\downarrow}}^{\dagger}\sigma_{\Omega_{01}^{\downarrow}} + a_{\Omega_{01}^{\downarrow}}\sigma_{\Omega_{01}^{\downarrow}}^{\dagger}\right)\right. \end{aligned}$$

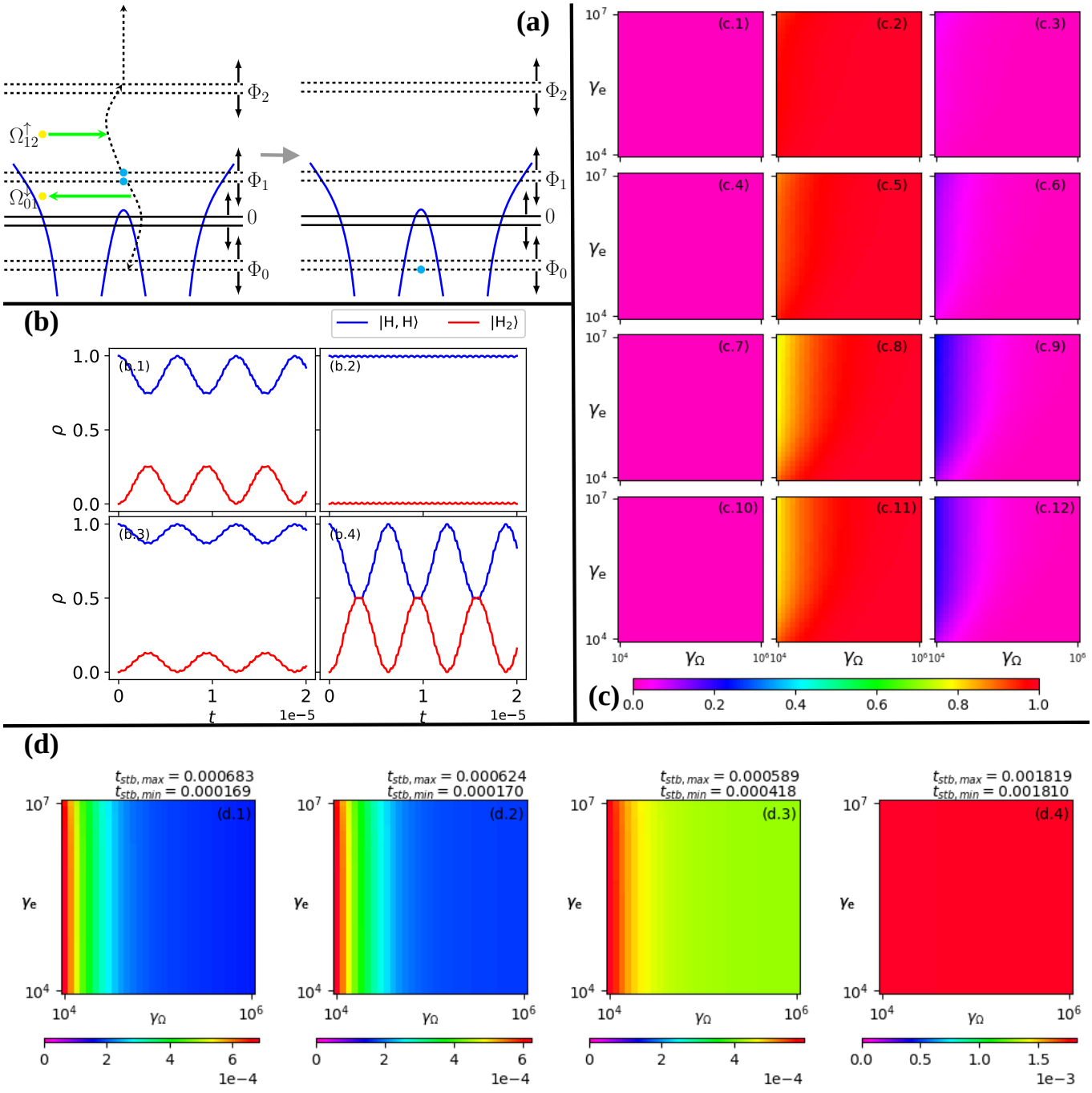

FIG. 1. (online color) *Ionization dynamics in a hydrogen molecule: unitary vs. dissipative evolution.* Panel (a) depicts the ionization process of a hydrogen molecule. Here, the blue and yellow dots, respectively, stand for electrons and photons. Panel (b) shows the unitary evolution under different initial conditions: (b.1) for initial states $|\Psi^0_{initial}\rangle$, $|\Psi^1_{initial}\rangle$, $|\Psi^2_{initial}\rangle$, $|\Psi^3_{initial}\rangle$, and $|\Psi^4_{initial}\rangle$; (b.2) for $|\Psi^5_{initial}\rangle$; (b.3) for $|\Psi^6_{initial}\rangle$; (b.4) for $|\Psi^7_{initial}\rangle$. Panel (c) shows the effect of different particle dissipation intensities on the ionization model (initial state is $|\Psi^6_{initial}\rangle$): the horizontal and vertical axes of each subpanel represent the γ_Ω and γ_e, respectively; the first through fourth rows correspond to γ_ω of 10^7, $10^{7.5}$, 10^8, and $10^{8.5}$, respectively; the first through third columns correspond to probabilities of $|\mathrm{H,H}\rangle$, $|\mathrm{H_2}\rangle$, and $|\mathrm{H_2^+}\rangle$, respectively. Here, the color bar for each heatmap ranges from 0 to 1. Panel (d) compares the time it takes for the system to reach a stable state: the four subpanels correspond to γ_ω of 10^7, $10^{7.5}$, 10^8, and $10^{8.5}$, respectively. Here, the color bar for each heatmap is scaled from 0 to the maximum value.

$$+ g_{\Omega_{12}^{\uparrow}} \left(a_{\Omega_{12}^{\uparrow}}^{\dagger} \sigma_{\Omega_{12}^{\uparrow}} + a_{\Omega_{12}^{\uparrow}} \sigma_{\Omega_{12}^{\uparrow}}^{\dagger} \right)$$
$$+ g_{\Omega_{12}^{\downarrow}} \left(a_{\Omega_{12}^{\downarrow}}^{\dagger} \sigma_{\Omega_{12}^{\downarrow}} + a_{\Omega_{12}^{\downarrow}} \sigma_{\Omega_{12}^{\downarrow}}^{\dagger} \right) \Big] \sigma_{\omega} \sigma_{\omega}^{\dagger}, \quad (7c)$$

$$H_{\text{bond}} = \hbar\omega a_{\omega}^{\dagger} a_{\omega} + \hbar\omega \sigma_{\omega}^{\dagger} \sigma_{\omega} + g_{\omega} \left(a_{\omega}^{\dagger} \sigma_{\omega} + a_{\omega} \sigma_{\omega}^{\dagger} \right), \quad (7d)$$

$$H_{\text{tun}} = \zeta \left(\sigma_n^{\dagger} \sigma_n + \sigma_n \sigma_n^{\dagger} \right) \sigma_{\omega}^{\dagger} \sigma_{\omega}, \quad (7e)$$

where $\hbar = h/2\pi$ is the reduced Planck constant, g is the coupling strength between the photon or phonon (with annihilation and creation operators a and $a^{\dagger}$, respectively) and the electron in the molecule (with excitation and relaxation operators $\sigma^{\dagger}$ and σ, respectively): $g_{\Omega_{01}^{\uparrow}}$ is the coupling strength for the photon mode $\Omega_{01}^{\uparrow}$, $g_{\Omega_{01}^{\downarrow}}$ is the coupling strength for the photon mode $\Omega_{01}^{\downarrow}$, $g_{\Omega_{12}^{\uparrow}}$ is the coupling strength for the photon mode $\Omega_{12}^{\uparrow}$, $g_{\Omega_{12}^{\downarrow}}$ is the coupling strength for the photon mode $\Omega_{12}^{\downarrow}$, g_{ω} is the strength of formation or breaking of covalent bond, ζ is the tunneling strength. $\sigma_{\omega}\sigma_{\omega}^{\dagger}$ verifies that covalent bond is formed, and $\sigma_{\omega}^{\dagger}\sigma_{\omega}$ verifies that covalent bond is broken.

It is known that the ionization of a hydrogen molecule requires pumping photons with a mode of Ω_{12} ($\Omega_{12}^{\uparrow}$ or $\Omega_{12}^{\downarrow}$) into the system to promote electron transition to an unstable transitional orbital. Therefore, we postulate the following three initial conditions:

- When the number of photons of mode Ω_{12} in the system is 1, i.e. $p_1 + p_2 = 1$. This gives us three configurations:
  1. $\{p_1 = 1,\ p_2 = 0\}$;
  2. $\{p_1 = 0,\ p_2 = 1\}$;
  3. Due to quantum superposition, we also consider their coherent and equally weighted superposition state: $\frac{1}{\sqrt{2}}\{p_1 = 1,\ p_2 = 0\} + \frac{1}{\sqrt{2}}\{p_1 = 0,\ p_2 = 1\}$.
- When the number of photons of mode Ω_{12} in the system is 2, i.e. $p_1 + p_2 = 2$. This gives us four configurations:
  1. $\{p_1 = 2,\ p_2 = 0\}$;
  2. $\{p_1 = 0,\ p_2 = 2\}$;
  3. $\{p_1 = 1,\ p_2 = 1\}$;
  4. Due to quantum superposition, we also consider their coherent superposition state: $\frac{1}{2}\{p_1 = 2,\ p_2 = 0\} + \frac{1}{2}\{p_1 = 0,\ p_2 = 2\} + \frac{1}{\sqrt{2}}\{p_1 = 1,\ p_2 = 1\}$, which indicates that the probability of having two photons of same mode $\Omega_{12}^{\uparrow}$ (or $\Omega_{12}^{\downarrow}$) in the system is $\frac{1}{4}$, whereas the probability of having one photon of mode $\Omega_{12}^{\uparrow}$ and another of mode $\Omega_{12}^{\downarrow}$ is $\frac{1}{2}$.
- When the number of photons of mode Ω_{12} in the system is 0, i.e., $\{p_1 = 0,\ p_2 = 0\}$.

Therefore, we obtain eight initial states

$$|\Psi_{initial}^{0}\rangle = |1\rangle|0\rangle \otimes |\Psi_f\rangle, \quad (8a)$$
$$|\Psi_{initial}^{1}\rangle = |0\rangle|1\rangle \otimes |\Psi_f\rangle, \quad (8b)$$
$$|\Psi_{initial}^{2}\rangle = \left(\frac{1}{\sqrt{2}}|1\rangle|0\rangle + \frac{1}{\sqrt{2}}|0\rangle|1\rangle \right) \otimes |\Psi_f\rangle, \quad (8c)$$
$$|\Psi_{initial}^{3}\rangle = |2\rangle|0\rangle \otimes |\Psi_f\rangle, \quad (8d)$$
$$|\Psi_{initial}^{4}\rangle = |0\rangle|2\rangle \otimes |\Psi_f\rangle, \quad (8e)$$
$$|\Psi_{initial}^{5}\rangle = |1\rangle|1\rangle \otimes |\Psi_f\rangle, \quad (8f)$$
$$|\Psi_{initial}^{6}\rangle = \left(\frac{1}{2}|2\rangle|0\rangle + \frac{1}{2}|0\rangle|2\rangle + \frac{1}{\sqrt{2}}|1\rangle|1\rangle \right) \otimes |\Psi_f\rangle, \quad (8g)$$
$$|\Psi_{initial}^{7}\rangle = |0\rangle|0\rangle \otimes |\Psi_f\rangle, \quad (8h)$$

where the first two qubits correspond to the $|p_1\rangle_{\Omega_{12}^{\uparrow}}|p_2\rangle_{\Omega_{12}^{\downarrow}}$ in Eq. (3), while the remaining qubits, being fixed, are collectively denoted as $|\Psi_f\rangle$, which is written as follows

$$|\Psi_f\rangle = |0\rangle|0\rangle|0\rangle|1\rangle|1\rangle \otimes \frac{1}{2}\left(|0\rangle|0\rangle - |0\rangle|1\rangle + |1\rangle|0\rangle - |1\rangle|1\rangle \right), \quad (9)$$

where the first three qubits $|0\rangle|0\rangle|0\rangle$ correspond to the $|p_3\rangle_{\Omega_{01}^{\uparrow}}|p_4\rangle_{\Omega_{01}^{\downarrow}}|p_5\rangle_{\omega}$ in Eq. (3), and shows that the number of photon of mode $\Omega_{01}^{\uparrow}$, the number of photon of mode $\Omega_{01}^{\downarrow}$, and the number of phonon of mode ω all equal to 0; the forth qubit $|1\rangle$ corresponds to $|L\rangle_b$, and indicates the break of the covalent bond; the fifth qubit $|1\rangle$ corresponds to $|k\rangle_n$, and indicates the state of nuclei, scattering in different cavities. We now focus on the last two qubits corresponding to the electronic states $|l_1\rangle_{e^{\uparrow}}|l_2\rangle_{e^{\downarrow}}$. Given that $L = 1$ and $k = 1$, the initial state is defined as having no covalent bond formed, and with the two hydrogen atoms located in separate cavities. Consequently, the electrons reside in their atomic orbitals. Assuming each atom carries one electron with opposite spins, we denote this electronic state as $|0_1\rangle|0_2\rangle$. According to Eq. (2), $|0_1\rangle|0_2\rangle$ can be written as

$$\begin{aligned} |0_1\rangle|0_2\rangle &= \frac{1}{\sqrt{2}}\left(|\Phi_0\rangle + |\Phi_1\rangle \right) \otimes \frac{1}{\sqrt{2}}\left(|\Phi_0\rangle - |\Phi_1\rangle \right) \\ &= \frac{1}{2}\left(|\Phi_0\rangle|\Phi_0\rangle - |\Phi_0\rangle|\Phi_1\rangle + |\Phi_1\rangle|\Phi_0\rangle - |\Phi_1\rangle|\Phi_1\rangle \right) \\ &= \frac{1}{2}\left(|0\rangle|0\rangle - |0\rangle|1\rangle + |1\rangle|0\rangle - |1\rangle|1\rangle \right). \end{aligned} \quad (10)$$

III. NUMERICAL RESULTS

A. Numerical method

The solution $\rho(t)$ in Eq. (4) may be approximately found as a sequence of two steps: in the first step we make one step in the solution of the unitary part of Eq.

(4)

$$\tilde{\rho}\left(t+dt\right)=exp\left(-\frac{i}{\hbar}Hdt\right)\rho\left(t\right)exp\left(\frac{i}{\hbar}Hdt\right). \quad (11)$$

And in the second step, make one step in the solution of Eq. (4) with the commutator removed

$$\rho\left(t+dt\right)=\tilde{\rho}\left(t+dt\right)+\frac{1}{\hbar}L\left(\tilde{\rho}(t+dt)\right)dt. \quad (12)$$

Evidently, computing the matrix exponential in Eq. (11) is a key step. While several classical mathematical methods have been proposed [37, 38] for this purpose, in this paper the precise time step integration method (PTSIM) [39–43] of matrix exponential is introduced. When solving the equations of motion using stepwise integration, the matrix exponential operation involved is $e^{A\Delta t}$. According to the addition theorem of matrix exponential

$$e^{A\Delta t}=\left[e^{A\frac{\Delta t}{2^M}}\right]^{2^M}=\left[e^{A\varepsilon}\right]^{2^M}, \quad (13)$$

where A is matrix, Δt is time step, $\varepsilon=\frac{\Delta t}{2^M}$ (usually M is taken to be equal to 20). The matrix exponential can be approximated using Taylor series expansion (4 terms)

$$e^{A\varepsilon}\approx I+A\varepsilon+\frac{(A\varepsilon)^2}{2!}+\frac{(A\varepsilon)^3}{3!}+\frac{(A\varepsilon)^4}{4!}, \quad (14)$$

where I is unit matrix, then

$$\begin{aligned}e^{A\Delta t}&\approx\left[I+A\varepsilon+\frac{(A\varepsilon)^2}{2!}+\frac{(A\varepsilon)^3}{3!}+\frac{(A\varepsilon)^4}{4!}\right]^{2^M}\\&=\left[I+T_{a,0}\right]^{2^M},\end{aligned} \quad (15)$$

where $T_{a,0}=A\varepsilon+\frac{(A\varepsilon)^2}{2!}+\frac{(A\varepsilon)^3}{3!}+\frac{(A\varepsilon)^4}{4!}$, then

$$\begin{aligned}\left[I+T_{a,0}\right]^{2^M}&=\left[(I+T_{a,0})^2\right]^{2^{M-1}}\\&=\left[I+2T_{a,0}+T_{a,0}T_{a,0}\right]^{2^{M-1}}\\&=\left[I+T_{a,1}\right]^{2^{M-1}}\\&=\left[I+T_{a,2}\right]^{2^{M-2}}\\&\cdots\cdots\\&=\left[I+T_{a,M}\right],\end{aligned} \quad (16)$$

where $T_{a,n}=2T_{a,n-1}+T_{a,n-1}T_{a,n-1},\ n\geq 1$. The above calculation process avoids operations between values with large differences in magnitude and avoids the impact of rounding errors.

B. Subspaces

Prior to analyzing the results, we first establish the definitions of three following subspaces

$$|\mathrm{H,H}\rangle=\sum_{L=1}|\cdots\rangle|L\rangle_b|\cdots\rangle, \quad (17a)$$

$$|\mathrm{H_2}\rangle=\sum_{L=0,k=0,AND(l_1\neq\varnothing,l_2\neq\varnothing)}|\cdots\rangle|L\rangle_b|k\rangle_n|l_1\rangle_{e^\uparrow}|l_2\rangle_{e^\downarrow}, \quad (17b)$$

$$|\mathrm{H_2^+}\rangle=\sum_{L=0,k=0,XOR(l_2=\varnothing,l_2=\varnothing)}|\cdots\rangle|L\rangle_b|k\rangle_n|l_1\rangle_{e^\uparrow}|l_2\rangle_{e^\downarrow}, \quad (17c)$$

where qubits without conditional restrictions are denoted by $|\cdots\rangle$. We partition the total Hilbert space into three subspaces, each corresponding to a distinct system state:

- Subspace $|\mathrm{H,H}\rangle$: Two independent hydrogen atoms ($L=1$ signifies no covalent bond formation).
- Subspace $|\mathrm{H_2}\rangle$: A neutral hydrogen molecule ($L=0$ signifies covalent bond formation; $k=0$ signifies both atoms are in the same cavity. The AND logical operator requires both $l_1\neq\varnothing$ and $l_2\neq\varnothing$).
- Subspace $|\mathrm{H_2^+}\rangle$: A hydrogen molecular cation ($L=0$ signifies covalent bond formation; $k=0$ signifies both atoms are in the same cavity. The XOR logical operator requires that either $l_1=\varnothing$ or $l_2=\varnothing$, but not both).

Eq. (17) presents a simplified form that lacks reduction factors. In practice, as we employ the Lindblad master equation (Eqs. (11) and (12)) which acts on the density matrix ρ, the diagonal elements of ρ represent probabilities. Thus, the probabilities for $|\mathrm{H,H}\rangle$, $|\mathrm{H_2}\rangle$, and $|\mathrm{H_2^+}\rangle$ are obtained by summing their respective associated diagonal elements.

C. Unitary evolution

We first consider an ideal, closed system where no particle inflow or escape occurs, meaning parameters γ_k and $\gamma_{k'}$ in Eq. (4) are set 0. Under this condition, the Lindblad master equation reduces to the von Neumann equation

$$i\hbar\dot{\rho}=\left[H,\rho\right]. \quad (18)$$

In the closed system, the absence of electron escape restricts the dynamics to oscillations between $|\mathrm{H,H}\rangle$ and $|\mathrm{H_2}\rangle$. We investigated the influence of eight different initial states on these oscillations, with the results presented in Fig. 1 (b). In subpanel (b.1), we observe that the oscillation curves for initial states $|\Psi^0_{initial}\rangle\sim|\Psi^4_{initial}\rangle$ completely coincide. This is because photons of mode $\Omega^\uparrow_{12}$ and $\Omega^\downarrow_{12}$ are energetically degenerate. Therefore, at the initial time and under otherwise identical conditions, pumping in one photon of mode $\Omega^\uparrow_{12}$ ($|\Psi^0_{initial}\rangle$) or one photon of mode $\Omega^\downarrow_{12}$ ($|\Psi^1_{initial}\rangle$) results in identical dynamics. Furthermore, the coherent, equal-weight superposition of states $|\Psi^0_{initial}\rangle$ and $|\Psi^1_{initial}\rangle$ ($|\Psi^2_{initial}\rangle$) also produces the same curve. Since the system contains only

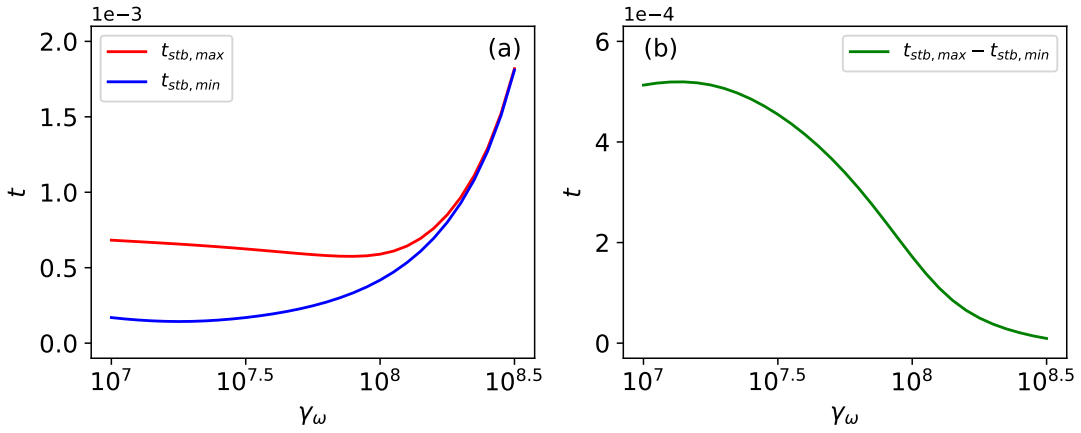

FIG. 2. (online color) *Comparison of the time it takes for the system to reach a stable state.* As shown in Fig. 1 (d), we investigated the impact of γ_Ω and γ_e on the system's stabilization time for $\gamma_\omega = 10^7$, $10^{7.5}$, 10^8, and $10^{8.5}$, identifying the maximum and minimum times for each case. We then analyzed how these extreme values evolve as γ_ω increases from 10^7 to $10^{8.5}$ (panel (a)). Additionally, the difference between them is plotted against γ_ω in panel (b).

one spin-up electron, the oscillation curve remains identical whenever the population of photons of mode $\Omega_{12}^{\uparrow}$ is greater than or equal to 1. Consequently, the curve for $|\Psi_{initial}^3\rangle$ coincides with that of $|\Psi_{initial}^0\rangle$, and by the same reasoning, the curve for $|\Psi_{initial}^4\rangle$ coincides with that of $|\Psi_{initial}^1\rangle$, too. For the initial state $|\Psi_{initial}^5\rangle$, which contains a photon of mode $\Omega_{12}^{\uparrow}$ and a photon of mode $\Omega_{12}^{\downarrow}$, both electrons with opposite spins have the opportunity to be excited into orbital Φ_2. Consequently, we obtain an oscillation curve distinct from those in (b.1), as shown in (b.2). Evidently, the superposition state of $|\Psi_{initial}^3\rangle$, $|\Psi_{initial}^4\rangle$, and $|\Psi_{initial}^5\rangle$ ($|\Psi_{initial}^6\rangle$) results from the combination of the two oscillation curves in subpanels (b.1) and (b.2), as shown in (b.3). Meanwhile, when there are neither photons of mode $\Omega_{12}^{\uparrow}$ nor photons of mode $\Omega_{12}^{\downarrow}$ initially ($|\Psi_{initial}^7\rangle$), the system exhibits an oscillation curve with the maximum amplitude, as shown in (b.4). From subpanels (b.1) to (b.4), we find that in the closed system, the excitation of electrons between orbital Φ_1 and orbital Φ_2 significantly reduces the amplitude of the oscillation curves.

D. Dissipative evolution

We now investigate the dissipative dynamics in the open system and the influence of different dissipation intensities on the formation of the H_2^+. We assume that two photons are pumped into the system randomly at the initial time, with equal probability for a photon of mode $\Omega_{12}^{\uparrow}$ and a photon of mode $\Omega_{12}^{\downarrow}$, resulting in the initial state $|\Psi_{initial}^6\rangle$. Due to the dissipative processes, the oscillations are damped, and the system eventually stabilizes after a sufficiently long evolution. The results in panel (c) of Fig. 1 show that the energy ultimately flows into two subspaces $|H_2\rangle$ and $|H_2^+\rangle$. Furthermore, electron dissipation intensities (γ_e) and phonon dissipation intensities (γ_ω) promote the formation of the hydrogen molecular cation, whereas photon dissipation intensities (γ_Ω) suppresses it. Our results consistently show that the population of $|H_2\rangle$ is significantly higher than that of $|H_2^+\rangle$ under all conditions, indicating the system's inherent tendency to form a stable neutral hydrogen molecule. For the time-based dynamic changes of the heatmap in panel (c), please refer to the video1.mp4.

In panel (c), we investigate the influence of γ_Ω and γ_e on $|H_2^+\rangle$ formation for $\gamma_\omega = 10^7$, $10^{7.5}$, 10^8, and $10^{8.5}$. We also determine the stabilization time t_{stb} for these four cases, defined as the time when the combined probability of $|H_2\rangle$ and $|H_2^+\rangle$ exceeds 0.999, and present the results as heatmaps in panel (d). The data reveal that γ_Ω significantly accelerates stabilization, whereas γ_e has a negligible effect. This is because the system evolves toward the stable hydrogen molecule, a process promoted by γ_Ω. Consequently, a larger γ_Ω leads to faster stabilization. Furthermore, as γ_ω increases, the difference between the maximum value $t_{stb,max}$ and minimum value $t_{stb,min}$ in the heatmaps decreases. This indicates that the promoting effect of γ_Ω becomes less pronounced at high γ_ω values. Fig. 2 plots $t_{stb,max}$ and $t_{stb,min}$ against γ_ω. Panel (a) of Fig. 2 shows that $t_{stb,max}$ decreases slowly from $\gamma_\omega = 10^7$ to 10^8, beyond which it increases exponentially. In contrast, $t_{stb,min}$ begins to rise at $\gamma_\omega < 10^{7.5}$. As shown in panel (b) of Fig. 2, the difference between $t_{stb,max}$ and $t_{stb,min}$ rapidly decreases to 0 with increasing γ_ω. This indicates that for $\gamma_\omega > 10^8$, the influence of γ_ω on t_{stb} is far greater than that of γ_Ω and γ_e.

As can be seen from Fig. 1 (c), the probability of obtaining the hydrogen molecular cation reaches its maxi-

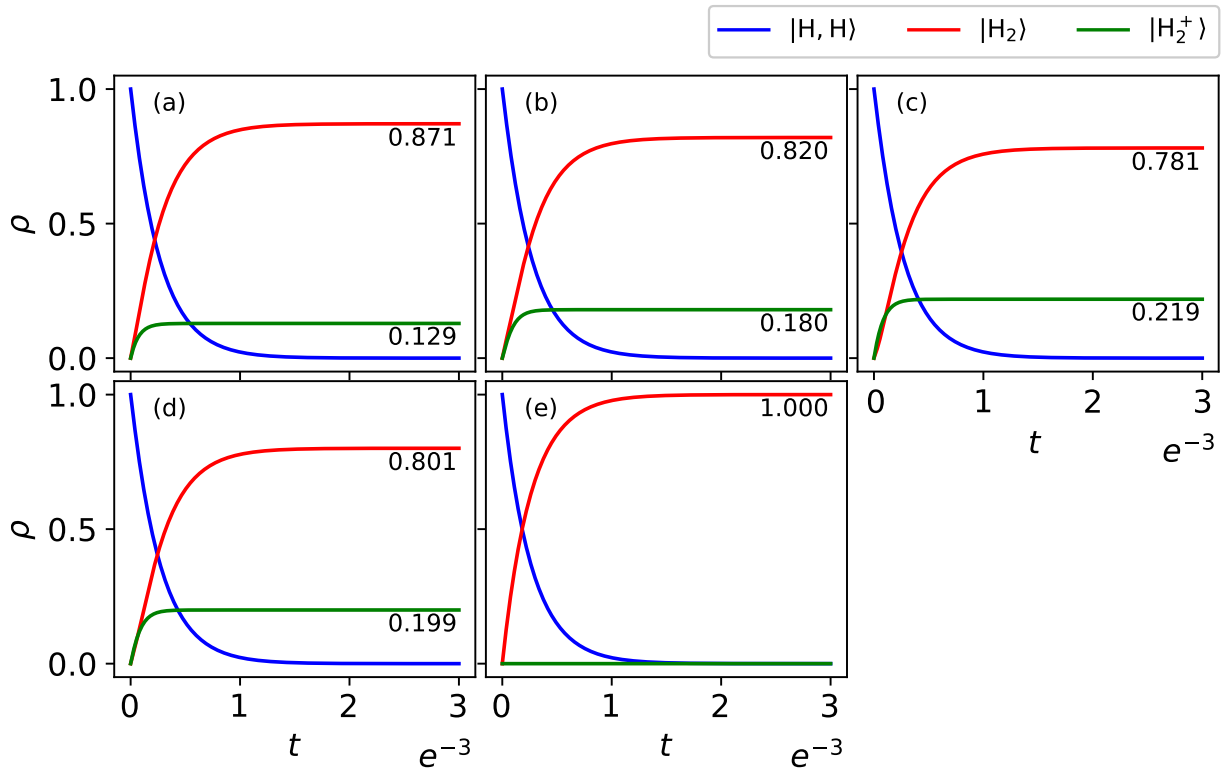

FIG. 3. (online color) *Dissipative dynamics for different initial conditions.* Panel (a) for $|\Psi^0_{initial}\rangle$, $|\Psi^1_{initial}\rangle$, $|\Psi^2_{initial}\rangle$; panel (b) for $|\Psi^3_{initial}\rangle$, $|\Psi^4_{initial}\rangle$; panel (c) for $|\Psi^5_{initial}\rangle$; panel (d) for $|\Psi^6_{initial}\rangle$; panel (e) for $|\Psi^7_{initial}\rangle$.

mum when γ_Ω is at its minimum ($\gamma_\Omega^{min} = 10^4$) while γ_ω and γ_e are at their maxima ($\gamma_\omega^{max} = 10^{8.5}$, $\gamma_e^{max} = 10^7$). Under these optimized conditions, we simulated the dissipative evolution of the system for different initial states, as shown in Fig. 3. In each panel, due to the presence of dissipation, the probability of $|\mathrm{H,H}\rangle$ gradually decays from 1 to 0. In the closed system, the unitary evolution from $|\Psi^0_{initial}\rangle$ to $|\Psi^4_{initial}\rangle$ is identical (see Fig. 1 (b)). In contrast, under dissipative evolution, the dynamics separate into two distinct cases, shown in Fig. 3 (a) and (b). Evidently, under dissipative evolution, the probability of obtaining the H_2^+ is higher for initial states $|\Psi^3_{initial}\rangle$ and $|\Psi^4_{initial}\rangle$ than for $|\Psi^0_{initial}\rangle$, $|\Psi^1_{initial}\rangle$, and $|\Psi^2_{initial}\rangle$. This is attributed to the fact that $|\Psi^3_{initial}\rangle$ ($|\Psi^4_{initial}\rangle$) contains two free photons of mode $\Omega^{\uparrow}_{12}$ ($\Omega^{\downarrow}_{12}$), whereas $|\Psi^0_{initial}\rangle$, $|\Psi^1_{initial}\rangle$, and $|\Psi^2_{initial}\rangle$ contain only one free photon of Ω_{12}. A greater population of these specific photons more effectively promotes the upward transition of electrons to the Φ_2 orbital, thereby facilitating the ionization of the hydrogen molecule. A comparison between panels (b) and (c) indicates that, for the same initial total photon number of two, an initial state comprising two photons of different modes ($\Omega^{\uparrow}_{12}$ and $\Omega^{\downarrow}_{12}$) is more effective at promoting hydrogen molecule ionization than a state with two photons of a single mode. This enhanced efficiency arises because state $|\Psi^5_{initial}\rangle$ can excite either a spin-up or a spin-down electron to the Φ_2 orbital. In contrast, $|\Psi^3_{initial}\rangle$ can only excite a spin-up electron, and $|\Psi^4_{initial}\rangle$ can only excite a spin-down electron. Furthermore, the characteristics of the annihilation operator used in the model constitute a second contributing factor to this observed difference. The matrix forms of the annihilation and creation operators are given by

$$a = \begin{array}{c} \\ |0\rangle \\ |1\rangle \\ |2\rangle \\ \vdots \\ \vdots \\ |p-2\rangle \\ |p-1\rangle \\ |p\rangle \end{array} \begin{array}{c} \begin{array}{cccccccc} |0\rangle & |1\rangle & |2\rangle & \cdots & \cdots & |p-2\rangle & |p-1\rangle & |p\rangle \end{array} \\ \begin{pmatrix} 0 & 1 & 0 & \cdots & \cdots & 0 & 0 & 0 \\ 0 & 0 & \sqrt{2} & \cdots & \cdots & 0 & 0 & 0 \\ 0 & 0 & 0 & \cdots & \cdots & 0 & 0 & 0 \\ \vdots & \vdots & \vdots & \ddots & \ddots & \vdots & \vdots & \vdots \\ \vdots & \vdots & \vdots & \ddots & \ddots & \vdots & \vdots & \vdots \\ 0 & 0 & 0 & \cdots & \cdots & 0 & \sqrt{p-1} & 0 \\ 0 & 0 & 0 & \cdots & \cdots & 0 & 0 & \sqrt{p} \\ 0 & 0 & 0 & \cdots & \cdots & 0 & 0 & 0 \end{pmatrix} \end{array}, \tag{19a}$$

$$a^\dagger = \begin{array}{c} \\ |0\rangle \\ |1\rangle \\ |2\rangle \\ \vdots \\ \vdots \\ |p-2\rangle \\ |p-1\rangle \\ |p\rangle \end{array} \begin{array}{c} \begin{array}{cccccccc} |0\rangle & |1\rangle & |2\rangle & \cdots & \cdots & |p-2\rangle & |p-1\rangle & |p\rangle \end{array} \\ \begin{pmatrix} 0 & 0 & 0 & \cdots & \cdots & 0 & 0 & 0 \\ 1 & 0 & 0 & \cdots & \cdots & 0 & 0 & 0 \\ 0 & \sqrt{2} & 0 & \cdots & \cdots & 0 & 0 & 0 \\ \vdots & \vdots & \vdots & \ddots & \ddots & \vdots & \vdots & \vdots \\ \vdots & \vdots & \vdots & \ddots & \ddots & \vdots & \vdots & \vdots \\ 0 & 0 & 0 & \cdots & \cdots & 0 & 0 & 0 \\ 0 & 0 & 0 & \cdots & \cdots & \sqrt{p-1} & 0 & 0 \\ 0 & 0 & 0 & \cdots & \cdots & 0 & \sqrt{p} & 0 \end{pmatrix} \end{array}. \tag{19b}$$

According to the aforementioned operators, when the particle number increases from $p-1$ to p or decreases from p to $p-1$, the corresponding parameter in the matrix is $\sqrt{p}$. This is manifested in the Lindblad master equation as a jump operator with a intensity of $\sqrt{p}\gamma$. Therefore, for initial states $|\Psi^3_{initial}\rangle$ and $|\Psi^4_{initial}\rangle$, the process of the photon number decreasing from 2 to 1 has a strength that is $\sqrt{2}$ times greater than that of the process from 1 to 0. This results in the two free photons in $|\Psi^3_{initial}\rangle$ and $|\Psi^4_{initial}\rangle$ being more likely to escape into the external environment at the initial stage compared to those in state $|\Psi^5_{initial}\rangle$. In panel (d), since state $|\Psi^6_{initial}\rangle$ is a superposition of states $|\Psi^3_{initial}\rangle$, $|\Psi^4_{initial}\rangle$, and $|\Psi^5_{initial}\rangle$, the resulting probability of obtaining the hydrogen molecular cation lies between the results shown in panel (b) and panel (c). In panel (e), since there are neither photons of mode $\Omega^{\uparrow}_{12}$ nor photons of mode $\Omega^{\downarrow}_{12}$ at the initial time, the ionization of the hydrogen molecule is forbidden.

E. Influx process

Having investigated the impact of dissipation on the system's evolution in Fig. 1 (c), we now turn to the effects of the influx process (see Fig. 4). First, we define the ratio of influx intensity to dissipative intensity as

$$\mu_k = \frac{\gamma_{k'}}{\gamma_k}, \tag{20}$$

where $\mu < 1$ indicates that the overall trend in the open system is dissipative, i.e., $\gamma_{k'} < \gamma_k$. According to Eq. (20), with the denominator held constant, the ratio is directly proportional to the numerator. Therefore, we can use μ_k directly to represent the $\gamma_{k'}$.

We now investigate the influx effect in the open system and the influence of different influx–dissipation ratios on the formation of the H_2^+. The initial state is $|\Psi^6_{initial}\rangle$. And the intensity of all dissipation channels is uniformly set to 10^7. Unlike in Fig. 1 (c), the results in Fig. 4 show that in some cases with influx effects, energy flows not only into subspaces $|H_2\rangle$ and $|H_2^+\rangle$, but is also partially retained in subspace $|H, H\rangle$. Only when $\mu_\omega = 0$ is the energy entirely channeled into $|H_2\rangle$ and $|H_2^+\rangle$ (see first row of panels in Fig. 4). Furthermore, the influx effect for photons promotes the formation of the H_2^+, whereas the influx effect for electrons suppresses it. Specifically, the influx effect for phonons suppresses the formation of the $|H_2\rangle$. However, it does not significantly promote the formation of the $|H_2^+\rangle$, but rather enhances the stability of two separate hydrogen atoms ($|H, H\rangle$). For the time-based dynamic changes of the heatmap in Fig. 4, please refer to the video2.mp4.

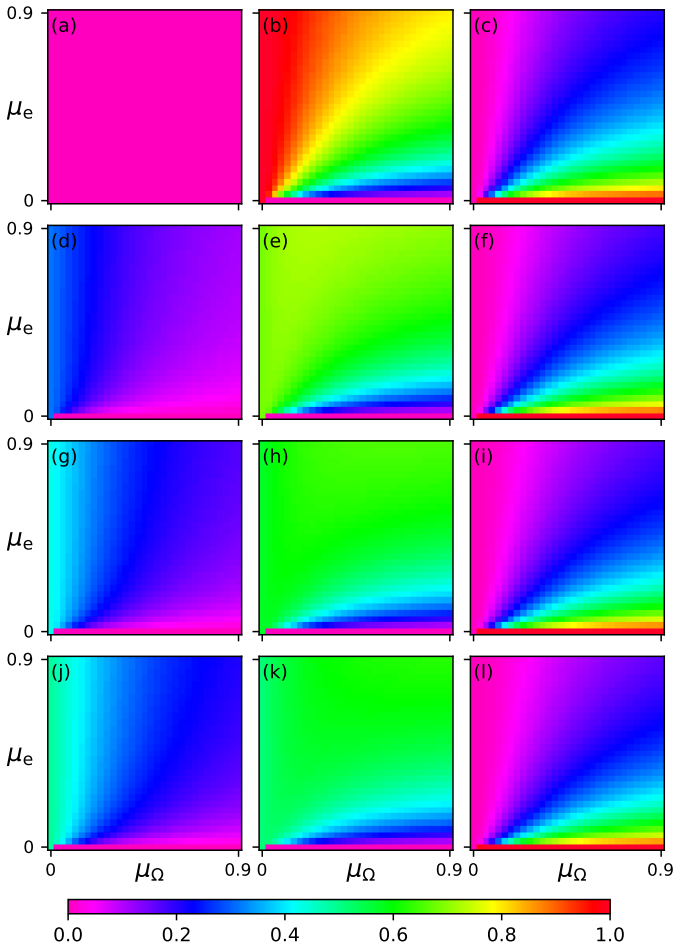

FIG. 4. (online color) *The influx effect.* Picture shows the effect of different particle influx intensities on the ionization model (initial state is $|\Psi^6_{initial}\rangle$): the horizontal and vertical axes of each panel represent the influx–dissipation ratio for photons (μ_Ω) and for electrons (μ_e), respectively; the first through fourth rows correspond to influx–dissipation ratio for phonons (μ_ω) of 0, 0.3, 0.6, and 0.9, respectively; the first through third columns correspond to probabilities of $|H, H\rangle$, $|H_2\rangle$, and $|H_2^+\rangle$, respectively. Here, the color bar for each heatmap ranges from 0 to 1.

F. Model with anode

Fig. 1 (b) presents the unitary evolution within the closed system. We now introduce a special model: an anode is incorporated into this closed system to adsorb electrons. The panel (a) in Fig. 5 shows when the electron occupies transitional orbital, it is highly susceptible to attraction by the positive electrode, enabling it to escape from the hydrogen molecule and thereby ionize the hydrogen molecule. The anode can absorb at most one electron. This is because the transition of an electron to the Φ_2 orbital can only occur when two electrons are present. When only one electron remains, the system's energy is lowered, making it less likely for the electron to escape the nuclear binding.

The dissipative evolution in this new model under different initial conditions is shown in Fig. 5 (b). Since only electrons can be absorbed, while photons and phonons

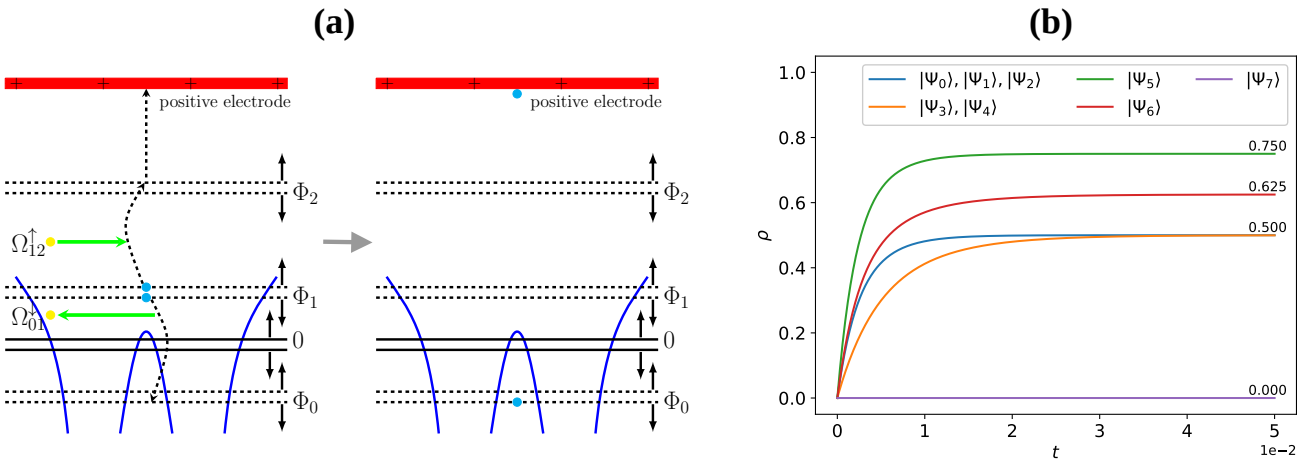

FIG. 5. (online color) *The model with an anode.* In panel (a), the hydrogen molecule is assumed to be in a perfectly isolated environment, preventing free particles from dissipating to the external system. However, electrons can be absorbed by an embedded anode, which is considered as electron escape. Panel (b) shows the time-dependent probabilities of the $|H_2^+\rangle$ under different initial conditions.

cannot escape, the system's energy can only flow towards subspace $|H_2^+\rangle$. Consequently, we can determine the maximum probability of the hydrogen molecular cation for different initial conditions. According to Eq. (10), when atomic orbitals hybridize into molecular orbitals, the spin-up electron has an equal probability of occupying the excited orbital (Φ_1) or the ground state orbital (Φ_0). This implies that a spin-up electron has only a $\frac{1}{2}$ chance of transitioning to the Φ_2 orbital for eventual absorption by the anode. The same logic applies to a spin-down electron. Based on this mechanism, the final probability of obtaining the hydrogen molecular cation is calculated as follows:

- For initial states $|\Psi^0_{initial}\rangle$ to $|\Psi^4_{initial}\rangle$, which involve only one type of free photon (where the photon number only affects the evolution speed, not the outcome), the probability is $\frac{1}{2}$.
- For $|\Psi^5_{initial}\rangle$, which contains both types of free photons, enabling both spin channels, the probability is $\frac{3}{4}$.
- For $|\Psi^6_{initial}\rangle$, which is a superposition of $|\Psi^3_{initial}\rangle$, $|\Psi^4_{initial}\rangle$, and $|\Psi^5_{initial}\rangle$, the resulting probability is derived as $\frac{5}{8}$.
- For $|\Psi^7_{initial}\rangle$, which contains no free photons, the probability is 0.

IV. CONCLUSION AND OUTLOOK

In this work, we have systematically investigated the quantum dynamics of hydrogen molecule ionization in closed quantum systems, as well as open quantum systems driven by dissipation and particle influx. Our key findings reveal that

- The system exhibits a strong tendency to form the stable neutral hydrogen molecule ($|H_2\rangle$) under a wide range of conditions.
- The interplay among dissipation channels (γ_Ω, γ_e, γ_ω) critically governs both the stabilization time and final state distribution, with γ_Ω acting as a key promoter of molecular stability and significantly accelerating the stabilization process.
- The introduction of particle influx (μ_k) leads to more complex energy partitioning, enabling population retention in the atomic state ($|H, H\rangle$) — a phenomenon absent in purely dissipative dynamics.
- The ionization pathway shows high sensitivity to the initial quantum state, particularly the composition and number of photons, which control the accessible excitation channels for electrons of different spins.
- These insights are further confirmed by an anode model, showing that the maximum ionization probability is fundamentally limited by orbital hybridization and initial state configuration, reaching a theoretical maximum of $\frac{3}{4}$ under optimal conditions.

Looking forward, several promising directions emerge from this study. First, extending our model to include non-Markovian environments would provide a more realistic description of systems where memory effects and coherent feedback from the environment are significant. Second, investigating more complex molecular systems,

such as heteronuclear diatomic molecules or those with more electrons, would test the generality of our findings and uncover new collective quantum effects. Finally, an experimental realization of this setup, for instance, using ultracold atoms in optical cavities or quantum simulator platforms, would be a critical step towards verifying our theoretical predictions and harnessing this quantum-controlled chemistry in practice.

ACKNOWLEDGMENTS

The study was funded by the China Scholarship Council, project number 202108090483. The author acknowledges the Center for Collective Use of Ultra-High-Performance Computing Resources (https://parallel.ru/) at Lomonosov Moscow State University for providing supercomputer resources that contributed to the research results.

[1] Q. Wang, H.-Y. Liu, Q.-S. Li, Y. Li, Y. Chai, Q. Gong, H. Wang, Y.-C. Wu, Y.-J. Han, G.-C. Guo, and G.-P. Guo, ChemiQ: A chemistry simulator for quantum computer (2021).

[2] J. R. McClean, N. C. Rubin, J. Lee, M. P. Harrigan, T. E. O'Brien, R. Babbush, W. J. Huggins, and H.-Y. Huang, What the foundations of quantum computer science teach us about chemistry, The Journal of Chemical Physics **155**, 150901 (2021).

[3] D. Claudino, A. J. McCaskey, and D. I. Lyakh, A backend-agnostic, quantum-classical framework for simulations of chemistry in C++, ACM Transactions on Quantum Computing **4**, 10.1145/3523285 (2022).

[4] J. Zhu, Quantum simulation of dissociative ionization of H_2^+ in full dimensionality with a time-dependent surface-flux method, Phys. Rev. A **102**, 053109 (2020).

[5] A. Vitaliy, K. Zheng, K. Alexei, H. Miao, O. Yuri, L. Wanshun, and V. Nadezda, About chemical modifications of finite dimensional QED models, Nonlinear Phenomena in Complex Systems **24**, 230 (2021).

[6] R. Chen, J. You, and Y. I. Ozhigov, Qualitative model of the hydrogen peroxide positive ion in a heat bath, Comput Math Model **33**, 408 (2022).

[7] H. hui Miao and Y. I. Ozhigov, Using a modified version of the Tavis–Cummings–Hubbard model to simulate the formation of neutral hydrogen molecule, Physica A: Statistical Mechanics and its Applications **622**, 128851 (2023).

[8] H.-h. Miao and Y. I. Ozhigov, Comparing the effects of nuclear and electron spins on the formation of neutral hydrogen molecule, Lobachevskii Journal of Mathematics **44**, 3111 (2023).

[9] J. You, R. Chen, W. Li, H. hui Miao, and Y. I. Ozhigov, Simulating and investigating various dynamic aspects of the h2o-related hydrogen bond model, Chinese Journal of Physics **97**, 753 (2025).

[10] I. I. Rabi, On the process of space quantization, Phys. Rev. **49**, 324 (1936).

[11] I. I. Rabi, Space quantization in a gyrating magnetic field, Phys. Rev. **51**, 652 (1937).

[12] R. H. Dicke, Coherence in spontaneous radiation processes, Phys. Rev. **93**, 99 (1954).

[13] J. J. Hopfield, Theory of the contribution of excitons to the complex dielectric constant of crystals, Phys. Rev. **112**, 1555 (1958).

[14] E. Jaynes and F. Cummings, Comparison of quantum and semiclassical radiation theories with application to the beam maser, Proceedings of the IEEE **51**, 89 (1963).

[15] M. Tavis and F. W. Cummings, Exact solution for an N-molecule—radiation-field Hamiltonian, Phys. Rev. **170**, 379 (1968).

[16] D. G. Angelakis, M. F. Santos, and S. Bose, Photon-blockade-induced mott transitions and XY spin models in coupled cavity arrays, Phys. Rev. A **76**, 031805 (2007).

[17] J. Casanova, G. Romero, I. Lizuain, J. J. García-Ripoll, and E. Solano, Deep strong coupling regime of the Jaynes–Cummings model, Phys. Rev. Lett. **105**, 263603 (2010).

[18] S. Haroche, Nobel lecture: Controlling photons in a box and exploring the quantum to classical boundary, Rev. Mod. Phys. **85**, 1083 (2013).

[19] X. Gu, A. F. Kockum, A. Miranowicz, Y. xi Liu, and F. Nori, Microwave photonics with superconducting quantum circuits, Physics Reports **718-719**, 1 (2017), microwave photonics with superconducting quantum circuits.

[20] P. Forn-Díaz, L. Lamata, E. Rico, J. Kono, and E. Solano, Ultrastrong coupling regimes of light-matter interaction, Rev. Mod. Phys. **91**, 025005 (2019).

[21] A. F. Kockum and F. Nori, Quantum bits with Josephson junctions, in *Fundamentals and Frontiers of the Josephson Effect*, edited by F. Tafuri (Springer International Publishing, Cham, 2019) pp. 703–741.

[22] A. Frisk Kockum, A. Miranowicz, S. De Liberato, S. Savasta, and F. Nori, Ultrastrong coupling between light and matter, Nature Reviews Physics **1**, 19 (2019).

[23] S. Prasad and A. Martin, Effective three-body interactions in Jaynes–Cummings–Hubbard systems, Sci Rep **8**, 16253 (2018).

[24] H. Wei, J. Zhang, S. Greschner, T. C. Scott, and W. Zhang, Quantum monte carlo study of superradiant supersolid of light in the extended Jaynes–Cummings–Hubbard model, Phys. Rev. B **103**, 184501 (2021).

[25] Y. Ozhigov, Quantum gates on asynchronous atomic excitations, Quantum Electron. **50**, 10.1070/QEL17320 (2020).

[26] K. C. Smith, A. Bhattacharya, and D. J. Masiello, Exact k-body representation of the Jaynes–Cummings interaction in the dressed basis: Insight into many-body phenomena with light, Phys. Rev. A **104**, 013707 (2021).

[27] R. Düll, A. Kulagin, L. Lee, Y. Ozhigov, H. Miao, and K. Zheng, Quality of control in the Tavis–Cummings–Hubbard model, Computational Mathematics and Modeling **32**, 75 (2021).

[28] H.-h. Miao, Investigating entropic dynamics of multi-qubit cavity QED system, Advanced Quantum Technologies **7**, 2400246 (2024).

[29] H. hui Miao and W. Li, Entanglement and quantum dis-

cord in the cavity QED model (2024).
[30] H.-h. Miao and Y. I. Ozhigov, Distributed computing quantum unitary evolution, Lobachevskii Journal of Mathematics **45**, 3121 (2024).
[31] W. Li, H.-h. Miao, and Y. I. Ozhigov, Supercomputer model of finite-dimensional quantum electrodynamics applications, Lobachevskii Journal of Mathematics **45**, 3097 (2024).
[32] R. Alicki, The quantum open system as a model of the heat engine, Journal of Physics A: Mathematical and General **12**, L103 (1979).
[33] H.-P. Breuer, F. Petruccione, *et al.*, *The theory of open quantum systems* (Oxford University Press, 2002).
[34] R. Kosloff, Quantum thermodynamics: A dynamical viewpoint, Entropy **15**, 2100 (2013).
[35] W. Pauli, Über den Zusammenhang des Abschlusses der Elektronengruppen im Atom mit der Komplexstruktur der Spektren, Zeitschrift fur Physik **31**, 765 (1925).
[36] Y. Wu and X. Yang, Strong-coupling theory of periodically driven two-level systems, Phys. Rev. Lett. **98**, 013601 (2007).
[37] C. Moler and C. Van Loan, Nineteen dubious ways to compute the exponential of a matrix, SIAM Review **20**, 801 (1978).
[38] C. Moler and C. Van Loan, Nineteen dubious ways to compute the exponential of a matrix, twenty-five years later, SIAM Review **45**, 3 (2003).
[39] W.-x. Zhong and Z.-s. Yang, On the computation of the main eigen-pairs of the continuous-time linear quadratic control problem, Applied Mathematics and Mechanics **12**, 45 (1991).
[40] Z. W X and W. F W, A precise time step integration method, Proceedings of the Institution of Mechanical Engineers, Part C: Journal of Mechanical Engineering Science **208**, 427 (1994).
[41] W.-x. Zhong, On precise time-integration method for structural dynamics (in Chinese), Journal of Dalian University of Technology **34**, 131 (1994).
[42] W.-x. Zhong, Precise integration for transient analysis (in Chinese), Computational Structure Mechanics and Applications **12**, 1 (1995).
[43] G. Qiang, T. ShuJun, and Z. WanXie, A survey of the precise integration method, SCIENTIA SINICA Technologica **46**, 1207 (2016).